Microfluid Nanofluid (2012) 13:451–459
DOI 10.1007/s10404-012-0973-z

RESEARCH PAPER

Fabrication of suspended electrokinetic microchannels from directly written sacrificial polymer fibers

Scott M. Berry · Thomas J. Roussel · Scott D. Cambron · Robert W. Cohn · Robert S. Keynton

Received: 24 February 2012 / Accepted: 26 March 2012 / Published online: 10 April 2012

Abstract Freely suspended microchannels with diameters ranging from 4 to 100 μm were fabricated by utilizing directly written PMMA fibers as sacrificial structures. These precisely oriented fibers served as scaffolds around which thin cylinders of glass were deposited (via sputtering), followed by a conformal coating of Parylene to augment the mechanical integrity of the structures. After coating, the PMMA fibers were dissolved to yield suspended, hollow conduits that were hydrophilic and robust. The freely suspended channels were loaded with a buffer solution containing charged particles, which were subsequently electrokinetically manipulated and velocities quantified using microparticle image velocimetry (μPIV). Mobilities within 1.3 % of those observed in conventional, planar microchannels were recorded.

Electronic supplementary material The online version of this article (doi:10.1007/s10404-012-0973-z) contains supplementary material, which is available to authorized users.

S. M. Berry · T. J. Roussel · S. D. Cambron · R. S. Keynton
Department of Mechanical Engineering,
University of Louisville, 200 Sackett Hall,
Louisville, KY 40292, USA
e-mail: Scott.Michael.Berry@gmail.com

S. M. Berry · R. W. Cohn · R. S. Keynton
The ElectroOptics Research Institute and Nanotechnology Center, University of Louisville, Louisville, KY 40292, USA

Present Address:
S. M. Berry
Department of Biomedical Engineering,
University of Wisconsin-Madison, 1111 Highland Ave.,
WIMR 6th Floor, Madison, WI 53726, USA

T. J. Roussel · S. D. Cambron · R. S. Keynton (✉)
Department of Bioengineering, University of Louisville,
419 Lutz Hall, Louisville, KY 40292, USA
e-mail: rob.keynton@louisville.edu

Keywords Microchannels · Suspended · Electroosmotic flow · Fabrication · Direct write

1 Introduction

Conventionally, microfluidic channels have been fabricated by selectively etching open troughs in substrate materials, including glass, silicon, and metal, and then bonding these substrates together to form hermetically sealed conduits (Hsu 2002). Alternatively, photolithography has been used to produce a negative "master copy" as a template for rapidly molding several identical microfluidic devices by utilizing processes such as polydimethylsiloxane (PDMS) casting and hot embossing of polymers (Anderson et al. 2000; Chiu et al. 2000, 2001; Jo et al. 2000). Unfortunately, because these techniques are all based upon traditional planar photolithography, the potential channel arrangement is quite limited as channels cannot be oriented in multilevel configurations.

More recently, techniques have emerged that enable the fabrication of three-dimensional microfluidic networks. Among the most popular of these methods is a process by which several planar polymer monoliths containing microchannels are fabricated by casting liquid polymer onto microfabricated master copies (Anderson et al. 2000; Jo et al. 2000). These individual layers are then precisely aligned with one another and stacked to form a multilayered, polymer-based microfluidic network. Jo et al. (2000) have employed this technique to fabricate a five-layer microfluidic device from thermally cured PDMS using a series of templates photolithographically fabricated from the photoresist, SU-8. Anderson et al. (2000) used "two-level photolithography" to construct masters with features at two distinct heights, thereby reducing the number of distinct layers required to fabricate a three-dimensional

microfluidic device. In this manner, a "basketweave" pattern, in which microchannels alternatively pass over and under one another without intersection, was produced from two layers of thermally cured PDMS. Similarly, Blanco et al. (2004) fabricated a two-level microfluidic device by photolithographically patterning channels into two thick films of SU-8 epoxy on silicon wafers and thermally bonding the two halves together.

Although most three-dimensional device fabrication strategies involve the accumulation of several two-dimensional layers, recent advances have enabled 3D microchannel formation via other processes. Hwang et al. (2004) have discovered that focused laser pulses can be used to selectively ablate material in a bulk glass substrate. This technique was employed to create channels with diameters measuring tens of microns, but with aspect ratios of only 40:1 or less. Previous work by our group utilized polymer fibers as sacrificial structures; fibers were coated with a metal or polymer layer, and then dissolved to produce a hollow channel (Harfenist et al. 2004). Similar processes have been reported by Verbridge et al. (2005), Kameoka et al. (2003), Czaplewski et al. (2004), and Bellan et al. (2009) in which electrospun materials were over-coated and then removed to yield hollow micro- and/or nanochannels. However, precise channel placement is not possible with these techniques due to the associated random fiber orientation.

The purpose of this investigation is to develop and validate a new process for producing precisely oriented networks of suspended microchannels. This capability will facilitate future production of complex microfluidic devices with multileveled, three-dimensional architectures. As the channels will be small in diameter and freely suspended, rather than embedded in a thick monolith, excessive stresses will be encountered by the microchannel walls when transporting liquid by traditional pressure-driven flow. Therefore, the interior wall of the microchannels will possess a surface charge in order to establish the electric double layer essential for electroosmotic flow while also enabling facile channel filling via capillary action. The fabrication of such channels will employ a direct-write process developed by our group (Berry et al. 2006, 2011a, b) and others (Nain et al. 2006) to generate suspended fibers that will act as sacrificial components in the production of microchannels. In the direct-write process, a viscous solution of poly(methyl methacrylate) (PMMA) is loaded into a micromanipulator-controlled syringe and drawn into suspended filaments. During direct-write drawing, capillary forces cause the polymer solution filament to thin as the solvent evaporates, ultimately resulting in a suspended fiber with a diameter in the order of a few microns (Berry et al. 2011a) (Fig. 1). Furthermore, past experimentation has demonstrated that fiber diameter is controllable through modulation of the solution properties

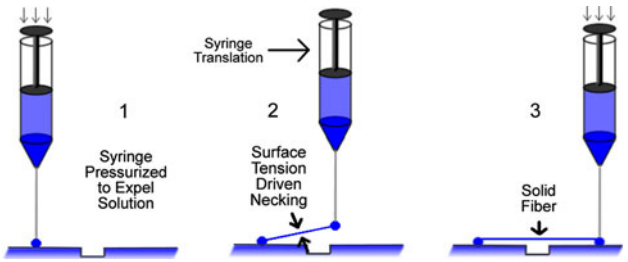

Fig. 1 Schematic of the direct-write process. *1* Pendant droplet is expelled into contact with the substrate. *2* Syringe translated to draw filament of solution, which thins via surface tension. *3* Establishment of a secondary contact point to complete fiber fabrication (modified from Berry et al. 2011a)

(viscosity, surface tension, evaporation rate of solvent) or the system geometry (fiber length, drawing rate) (Berry et al. 2006, 2011a; Nain et al. 2006).

2 Methodology

2.1 Fabrication overview

Pairs of square electrodes measuring 6 mm on a side were first fabricated on a 2-mm-thick soda lime glass plate using a photolithographic liftoff process. In this process, positive photoresist (Shipley 1813) was spun onto the plate and selectively patterned using UV light supplied by a maskless lithography system (Intelligent Micro Patterning). The various electrode metals were then deposited on top of the patterned resist via sputtering (Technics 4604) and patterned through liftoff of the resist in acetone. In order to demonstrate the suspended nature of the microchannel fabrication process, a trench measuring 500-μm wide and 500-μm deep was machined between each electrode pair via a dicing saw (Disco DAD 321, Tokyo, Japan).

Sacrificial polymer fibers were fabricated using the previously described direct-write method (Fig. 1) using a 25 % (by wt. %) solution of PMMA (MW = 996 kDa, Sigma-Aldrich, St. Louis, MO) dissolved in chlorobenzene. In brief, the polymer solution was loaded into a 1-mL syringe controlled by a micromanipulator. The syringe was pressurized to 25.3 psi to expel solution through a 22-gauge needle at a rate of approximately 20 μL/min. The micromanipulator was programmed to position the needle tip 500 μm above the surface of one electrode at a distance of 750 μm from the trench edge, such that the expelled pendant droplet of solution contacted the electrode. The syringe and needle were then moved 2 mm across the trench at a velocity of 20 mm/s to draw a filament of polymer solution spanning the trench as shown in Fig. 1.

The microchannels were created by sputter coating (RF sputtering, Technics 4604) the direct-write fibers with a

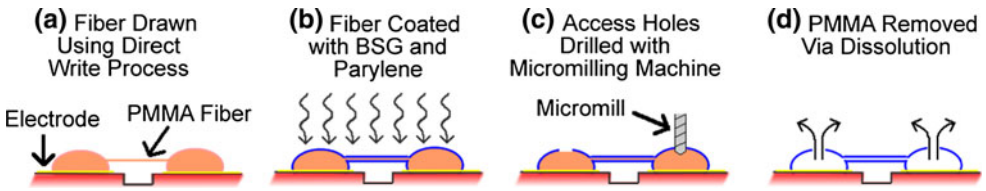

Fig. 2 Fabrication of channels from PMMA fibers. **a** PMMA fiber between two PMMA reservoirs on glass substrate with electrodes. **b** Deposition of BSG and parylene. **c** Drilling of 1-mm-diameter access holes to expose PMMA. **d** Removal of PMMA via dissolution

thin film ($t = 10$–85 nm) of borosilicate glass (BSG) to establish a hydrophilic inner channel wall. Due to the fragility of the BSG layer, a reinforcing outer wall ($t = 10$ μm) of Parylene was deposited using a room temperature, vapor-phase deposition technique (SCS Parylene Deposition System 2010, Indianapolis, IN). Additionally, an organo-silane compound (Silane A-174) was affixed to the BSG immediately prior to the vapor-phase deposition in order to promote adhesion between the BSG and Parylene. Following Parylene deposition, 1-mm-diameter access holes were drilled through the BSG and Parylene layers using an ultrahigh-precision micromilling machine (MMM) to provide access to the PMMA. These holes, which were positioned at each end of the coated fibers, enabled dissolution of the PMMA in acetone followed by critical point drying in liquid CO_2 of the remaining hollow structure (Fig. 2).

2.2 Characterization and optimization

Due to poor adhesion between the PMMA and gold electrodes during preliminary studies, a variety of other electrode materials were examined including copper, titanium, chromium, and platinum. These alternatives were evaluated not only on their adhesion with PMMA, but also their electrical conductivity and their ability to resist oxidation in an electrochemical setting. To test adhesion, several polymer fibers were drawn on each material using the direct-write method, inverted, and subjected to heat at 90 °C for 2 h to simulate the thermal and gravitational environment encountered during BSG sputtering. After heating, the percentage of PMMA fibers that were detached at either end were recorded and compared. Electrical conductivity was specified by Lide (1992), while electrochemical inertness was quantified by the oxidation potentials of the electrode materials, also specified by Lide (1992).

Polymer fibers created with the direct-write technique were coated with a thin layer of BSG that, upon removal of the polymer, became the hydrophilic inner layer of the microchannel wall. This layer was deposited by RF sputtering since uniform coverage around the circumference of the polymer fiber was required. However, due to the lack of literature regarding sputter coating of BSG on suspended, polymer microstructures, a characterization of this process was performed. One failure mechanism in this process originated from a mismatch in the coefficients of thermal expansion between the PMMA fibers ($\alpha = 70 \times 10^{-6}$ K^{-1}) and BSG ($\alpha = 3.3 \times 10^{-6}$ K^{-1}), which promoted buckling, cracking, and ultimately failure of the fragile BSG film essential to facilitate electro-osmotic (EO) flow (Fig. 3). To investigate this mechanism, BSG was sputtered on PMMA fibers at powers of 150 W and 300 W for durations ranging from 40 min to 240 min. The effect of layered deposition, with 20–40 min of cooling periods between layers, was also explored. The thicknesses of BSG films were measured with a profilometer (Dektak) and the overall quality of the films was evaluated through imaging with variable pressure scanning electron microscopy (VPSEM; Supra 35VP, Zeiss, Thornwood, NY).

Following deposition of the Parylene layer, profilometry was again utilized to determine the layer thickness. Additionally, selected channels were frozen in liquid nitrogen and cleaved with a razor blade in multiple locations along the channel length to expose the cross section of the microchannels. This area was imaged with the VPSEM to confirm the complete dissolution of the PMMA core while also verifying the smoothness and continuity of the BSG inner channel wall.

2.3 Microchannel operation

Multiple microchannels were filled with phosphate buffer solution (PBS, 10 mM, pH 6.1) loaded with 10μm-diameter fluorescent particles (Invitrogen F-8801, Duke Scientific R0100, or Sigma-Aldrich 90518) at a concentration of 0.1 % by volume. A range of electric fields (−80 to +80 V/cm) was applied between the electrodes to induce electroosmotic (EO) flow of the PBS solution and electrokinetic (EK) transport of the tracer particles. This motion was quantified using a microparticle image velocimetry (μPIV) system (TSI Inc., Shoreview, MN), interfaced with a fluorescent microscope (Zeiss Imager.D1) capable of directly imaging the microchannels. The particles were excited by dual Nd:YAG lasers (Quantel, Bozeman, MT) at 532 nm (120 mJ/pulse), controlled in

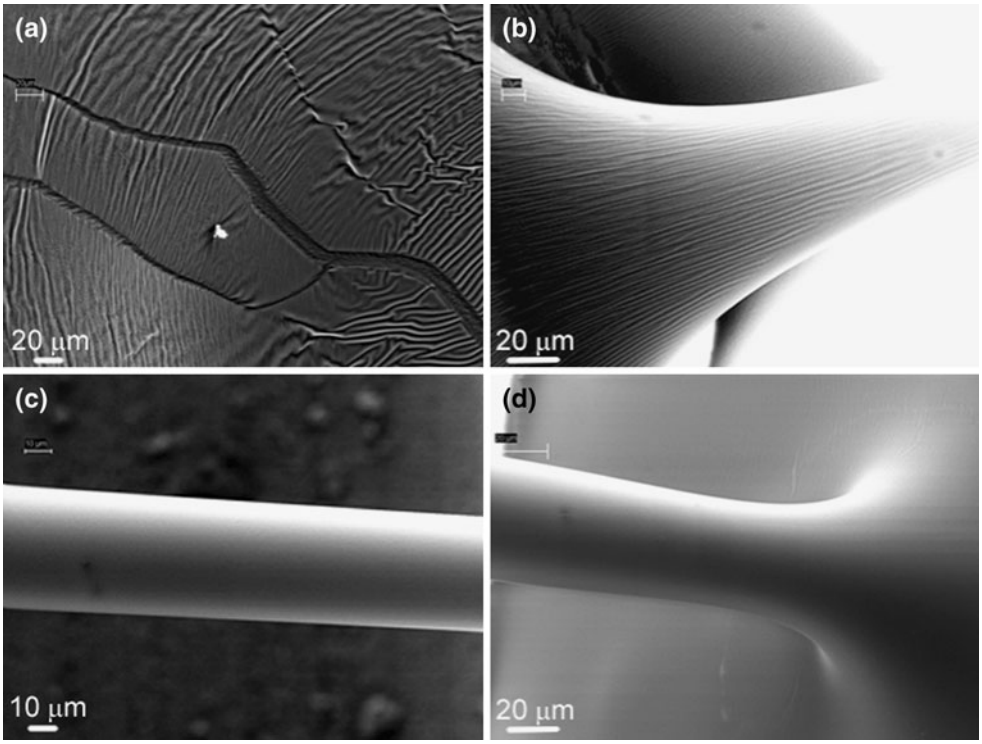

Fig. 3 BSG sputtered on PMMA at **a**, **b** 300 W for 40 min, **c** 150 W for 40 min, and **d** 3 layers at 150 W for 40 min each and 40 min cooling time between each layer

conjunction with a camera (TSI PowerView Plus) by a synchronizer (TSI 610035). This system was programmed to collect two fluorescent images (one from each laser pulse) in rapid succession (10–40 ms) such that the fluorescent particles had an average displacement of 10–20 pixels between images, thereby enabling the PIV software (TSI Insight 3G) to accurately track particle motion. Once raw image pairs (SI Figure 1a) were collected, they were processed, analyzed, and post-processed to determine the electrokinetic motion of the particles. First, all images of a particular sample were examined to determine the minimum signal at each pixel position common to all images. This "minimum signal image", representing the background light present for a specific sample, was subtracted from each pair to reduce background noise and enhance the signal-to-noise ratio of the particle fluorescence (SI Figure 1b). Next, a correlation algorithm was applied to each pair of images to calculate the particle motion (SI Figure 1c). Specifically, the images were partitioned into 128 × 128 pixel domains and processed using a recursive correlation algorithm that searched for similar partitions in both images within a user-defined radius, which was defined as 32 pixels based on the expected displacement of 10–20 pixels. Then, due to the recursive nature of this particular algorithm, the partitions were refined to 64 × 64 pixels and the correlation repeated to improve the resolution of the output. Using a 40× objective lens, this partition size resulted in a resolution of ~2 μm. Standard deviation validation was applied to remove all velocity vectors which differed by more than three standard deviations from their nearest neighbors, thereby reducing false correlations. In addition, smoothing validation was applied to fill in missing points of data by calculating a weighted average of all of the nearest neighboring locations (SI Figure 1d).

The total EK particle mobility measured by the PIV system is a superposition of the EO velocity of the fluid and the electrophoretic (EP) transport of the charged particles within the fluid, as indicated by:

$$\mu_{EK} = \mu_{EO} + \mu_{EP} \tag{1}$$

where μ_{EK}, μ_{EO}, and μ_{EP} are the EK, EO, and EP mobilities, respectively. Mobility is defined as:

$$\mu = VE \tag{2}$$

where V is velocity and E is the applied electric field strength. To decouple EO and EP, one of them must be isolated and measured independently without any significant alteration of its magnitude. A technique described by Hsieh et al. (2006) was employed in which the tracer particles in the buffer solution were loaded into an untreated (i.e., not plasma etched) PDMS channel formed by conventional soft lithography techniques. Because PDMS lacks a surface charge, EO mobility will be minimal ($\mu_{\oplus\not\in} < 1 \times 10^{-8}$ m^2/Vs) (Ren et al. 2001) relative to the magnitude of the total EK

mobility seen in preliminary trials ($\mu_{\oplus\supseteq} \approx 6 \times 10^{-8}$ m^2/Vs). This ability to isolate and quantify EP mobility enables the estimation of μ_{EO} within the BSG channels by subtracting the value of μ_{EP} (approximated by the apparent flow rate of the particles in the PDMS channels) from the value of μ_{EK} measured with the PIV using Eq. 1.

Measurements of μ_{EO} were validated through comparisons with the electroosmotic mobilities obtained by measuring fluid motion via PIV in similar-sized, glass microchannels. These microchannels were fabricated by milling microscale trenches (channel depths = 10–25 μm, channel widths = 35–100 μm, channel lengths = 2 mm) in a borosilicate glass wafer using the MMM equipped with a 25-μm-diameter end mill (Performance Micro Tool, Janesville, WI). The MMM was also employed to drill the 1-mm-diameter access holes at the ends of each channel. The trenches were sealed by attaching an untreated sheet of PDMS (Sylgard 184, Dow Corning, Midland, MI) over the trenches, thereby enclosing them. Sealed microchannels were then loaded with the fluorescent particle-doped buffer solution and PIV was used to quantify the EK motion of the particles.

3 Results and discussion

3.1 Fabrication

Preliminary attempts to fabricate microchannels connected to gold electrodes resulted in a very low yield (<10 %) of unbroken, hydrophilic channels. The most common cause of failure (47 % of the failed devices) was the delamination of the PMMA from the electrodes prior to or during the sputtering of the BSG layer. Quantification of electrode/PMMA fiber adhesion at 90 °C indicated that, of the five electrode materials tested, gold possessed the poorest adhesion characteristics (Table 1). This result agrees with past research by Khan Malek and Das (1998) stating that PMMA exhibits minimal adhesion to gold relative to other common metals such as copper and titanium. Furthermore, copper is unsuitable as an electrode material based on its susceptibility to oxidation in an electrochemical setting. Based on this data, platinum was chosen as the electrode material and was deposited via sputtering (DC sputtered at 120 W for 2 min) while utilizing a Ti adhesion layer (RF sputtered at 300 W for 1 min).

VPSEM imaging illustrated that attempts to deposit thin BSG layers at a high (300 W) sputtering power produced films that were undulating and cracked (Fig. 3a, b). Visual inspection of the samples revealed that the fibers themselves were noticeably deformed, suggesting that heat generated during the sputtering process may have elevated the temperature of the PMMA near or beyond its glass transition temperature (T_g = 105 °C). Smoother BSG films were observed when the sputtering power was reduced to 150 W (Fig. 3c), but the decreased film thicknesses (t = 8 nm) yielded devices that were detrimentally fragile. Robust, smooth BSG layers were successfully deposited via multilayered sputtering, in which BSG was deposited in thin (~10 nm) layers at low power while implementing a 40-min cooling period between each layer (Fig. 3d). Using this technique, smooth layers as thick as 80 nm were repeatably deposited on PMMA fibers. The necessity of the cooling phase between layers was confirmed when the

Table 1 Adhesion of PMMA fibers on electrode materials [conductivity and activity data from Lide (1992)]

Electrode material	Percentage detachment of PMMA from electrode (%)	Electrical conductivity (S/m)	Relative location in activity series (1 is most easily oxidized)
Gold	50	45.2×10^6	1
Chromium	24	8.0×10^6	3
Copper	30	59.6×10^6	4
Titanium	0	2.4×10^6	5
Platinum	0	9.52×10^6	2

Table 2 Outcomes of BSG sputtering processes

Sputtering power (W)	Sputtering time per layer (min)	Number of layers	Cooling time between layers (min)	BSG thickness (nm)	Film topology
300	40	1	NA	24	Cracked and buckled
150	40	1	NA	8	Smooth, but fragile
150	40	3	40	25	Smooth
150	40	6	20	85	Cracked and buckled
150	40	6	40	80	Smooth, very robust

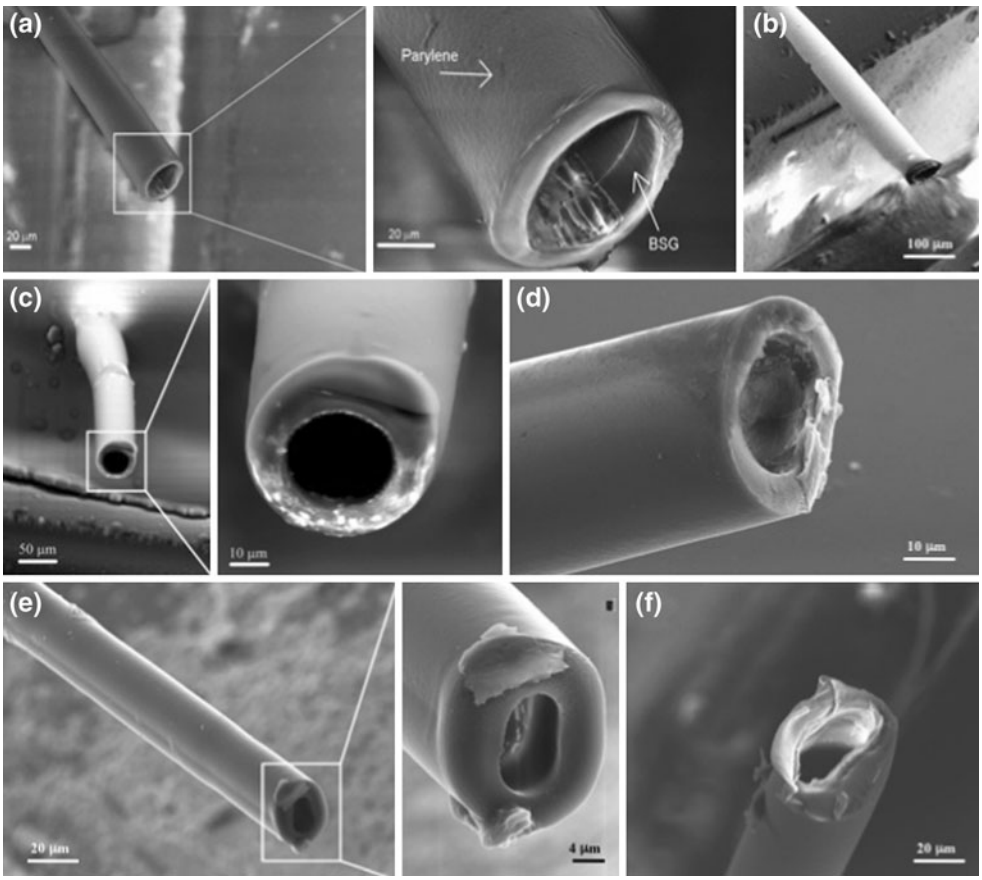

Fig. 4 Microchannels fabricated using direct-write fibers as sacrificial structures. **a** Cleaved 35-μm-diameter microchannel with inset highlighting BSG inner wall that partially delaminated from Parylene outer wall during cleaving, **b** cleaved 50-μm-diameter microchannel suspended over the edge of the trench, **c** cleaved 25-μm-diameter microchannel bent perpendicular to the electrode surface such that the base of the microchannel is visible, **d** cleaved 25-μm-diameter microchannel, **e** cleaved 7-μm-diameter microchannel with *inset* showing channel interior, and **f** cleaved 35-μm-diameter microchannel

cooling time was reduced to 20 min, where the cracked topology reemerged. Table 2 summarizes the outcomes of the various BSG sputtering processes.

Smooth layers of Parylene were deposited at a thickness of 10 ± 2 μm onto PMMA fibers coated with BSG as measured by profilometry. Access holes were drilled through the BSG and Parylene layers to expose the PMMA, which was entirely removed after 1 week in an acetone bath as confirmed by VPSEM images of cleaved microchannels (Fig. 4). Because the rate of dissolution of the PMMA was limited by the rate of diffusion of the solvent along the axis of the polymer fiber, a 7-day soak was implemented to ensure complete PMMA removal. In this manner, suspended microchannels with diameters ranging from 4 to 100 μm were fabricated between electrodes on either side of a 500-μm-wide trench (Fig. 5). Additionally, the process yield, defined as the percentage of fabrication attempts that

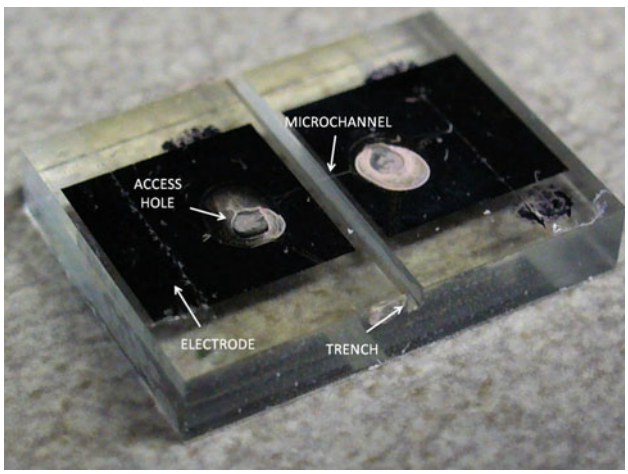

Fig. 5 Representative test chip employed to quantify EK mobility. The *bright regions* of material surrounding the access holes are desiccated droplets of fluorescent tracer particle solution

result in suspended, unbroken microchannels, was improved from preliminary levels of less than 10 % to over 80 %.

3.2 Operation

Microchannels were loaded with fluorescent particle-doped buffer (PBS, 10 mM, pH 6.1) by capillary action and EK transport was induced by applying a variety of electric fields (−80 to +80 V/cm) between the ends of the channel. The nature of the subsequent particle motion was observed to be strongly dependent on the type of particle loaded into the channel. Uncharged melamine particles (Sigma-Aldrich 90518) were found to strongly aggregate on the microchannel walls while moving toward the negative electrode, whereas slightly anionic polystyrene particles (Duke Scientific R0100) weakly adhered to the channel walls while moving toward the positive electrode. Only the strongly anionic, carboxylate-modified polystyrene particles (Invitrogen F8801) remained in suspension and did not immobilize on the channel wall while moving toward the positive electrode. This indicates that some degree of electrostatic repulsion between the negatively charged BSG channel wall and the tracer particles is required to obtain a flow profile that is unperturbed by particles binding to the sidewalls. Adsorption of positively charged (or uncharged) analytes to glass surfaces is a common problem encountered when performing EK experiments in glass capillaries. Often, this problem is overcome by functionalizing the interior of the microchannels (e.g., the attachment of a PEG monolayer to the channel interior via silane chemistry will

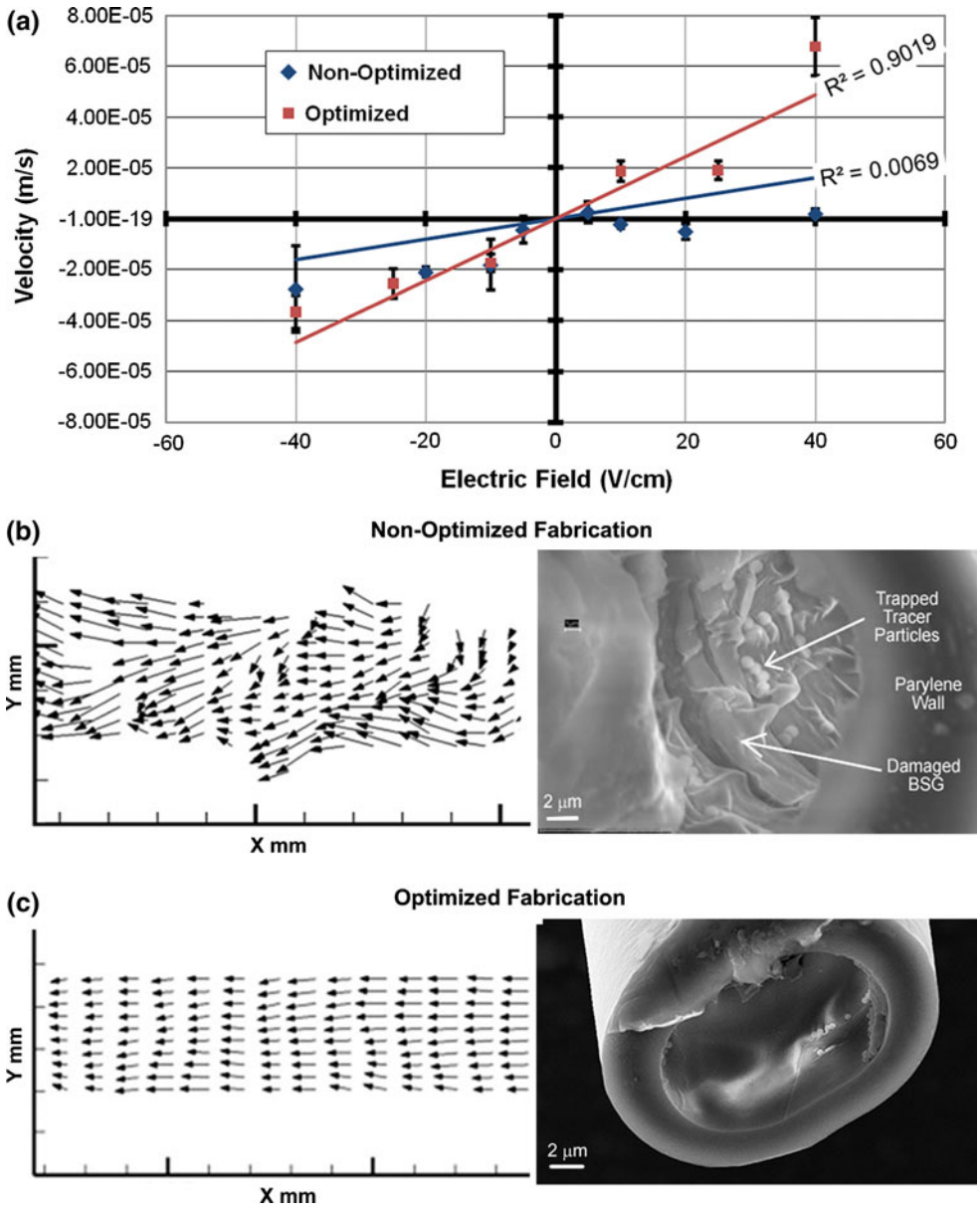

Fig. 6 a Comparison of particle velocity in optimized and non-optimized channels as a function of applied electric field. **b** (*Left*) erratic velocity profile in non-optimized microchannels and (*right*) SEM image of damaged interior of non-optimized channel after exposure to flow for 10 min. **c** (*Left*) smooth velocity profile observed in optimized channels and (*right*) SEM image of interior of optimized microchannel after exposure to flow for 10 min

significantly reduce adsorption) (Doherty et al. 2003). However, the focus of this study is the optimization of a new microchannel fabrication method, including the quality of a glass microchannel interior. Therefore, negatively charged, carboxylate-modified particles were exclusively utilized to quantify electrokinetic transport within the microchannels. The EP mobility of these particles was observed to be $+5.59 \times 10^{-8}$ m^2/Vs (toward the positive electrode) as determined by measurement of particle motion within untreated PDMS microchannels.

The velocities of the carboxylate-modified tracer particles were measured under a variety of electric fields ranging from -40 to $+40$ V/cm for multiple suspended microchannels fabricated under both ideal and non-ideal processing conditions. Increasing the magnitude of the electric field beyond 40 V/cm promoted the formation of channel-blocking bubbles via electrolysis of the buffer solution. EK mobility was determined by plotting the particle velocity as a function of electric field, then fitting a linear relationship to the data and extracting the slope of the line. Significant differences were observed between the microchannels with optimized BSG layers and those containing cracked or buckled BSG layers. Particle velocities in non-optimized microchannels did not linearly increase with increasing electric field as illustrated by the poor fit ($R^2 = 0.006$) of the linear regression in Fig. 6a. PIV data depicting a snapshot of flow within a non-optimal channel portrays a flow field that varies significantly from the uniform, "plug-type" flow generally encountered in electrokinetic transport. A potential source of these abundant localized perturbations is illustrated in Fig. 6b, which shows the cross section of a non-optimized microchannel after being exposed to electrokinetic flow for approximately 10 min. This image indicates that the cracked BSG layer has partially delaminated from the underlying Parylene, resulting in the multicausal impedance to electrokinetic transport, described as follows: (1) The delaminated BSG enters the flow stream, physically blocking or perturbing particle motion. (2) Gaps in the negative surface charge associated with the BSG layer prevent the formation of a continuous electric double layer (EDL), which is essential to EO flow. (3) Initial breaks in the BSG layer make the microchannels susceptible to breakdown at lower operating voltages, as described by Wolf and Tauber (1986).

The data given in Fig. 6b are in sharp contrast to the performance of microchannels fabricated with optimized, smooth BSG layers. Particle velocity increased relatively linearly ($R^2 = 0.901$) with increasing electric field, a characteristic trend of electrokinetic transport (Fig. 6a). Furthermore, the magnitude of velocity increased approximately threefold, suggesting that some of the factors impeding particle motion had been mitigated. Examination of a representative flow field snapshot (Fig. 6c) illustrates

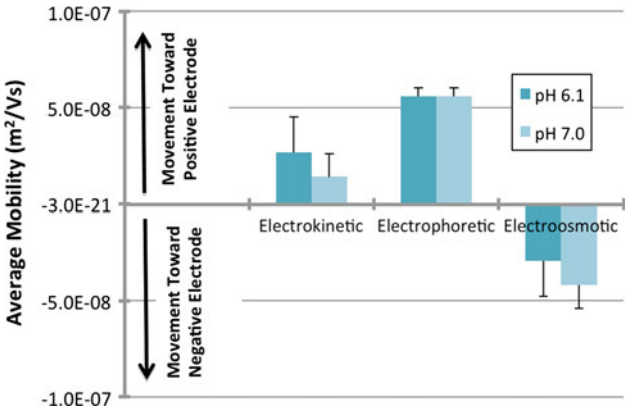

Fig. 7 EK, EP, and EO mobilities of flow in microchannels. Data represent velocity field data collected from four different microchannels with similar diameters (D = 20–35 μm) for each pH condition

that the particle velocity field resembles the expected "plug-type" flow, with a distinct reduction in velocity variance for the BSG-optimized microchannels. Finally, VPSEM imaging of the microchannel cross section (Fig. 6c) confirms the lack of cracks, buckles, and trapped particles in the optimized microchannels.

The average EK mobility was determined by calculating the slopes of the regression lines for the particle velocity versus electric field data in four different microchannels. EO mobility was calculated with Eq. 2 and it was observed that EO flow was directed toward the negative electrode, as is typical for EO flow in glass microchannels. In all cases, the bulk EK motion progressed toward the positive electrode, indicating that the EP motion of the particles possessed a larger magnitude than the EO flow of the buffer fluid (Fig. 7). The average EO mobility was found to be 2.92×10^{-8} m^2/Vs for a buffer of 10 mM, pH 6.1 and 4.18×10^{-8} m^2/Vs for a buffer of 10 mM, pH 7.0. These values compare relatively well with published values for similar PBS buffers [4.21×10^{-8} m^2/Vs with 10 mM buffer, pH 7.0 (Hsieh et al. 2006) and 3.87×10^{-8} m^2/Vs with 20 mM buffer, pH 6.3 (Carroll et al. 2008)] in conventionally fabricated glass microchannels. Furthermore, EO mobility in the suspended microchannels appears to follow the well-characterized relationship linking increasing buffer pH with increasing EO mobility (Beckers et al. 1991). Also, electrokinetic transport was induced in microchannels machined in BSG wafers, and it was discovered that the average electroosmotic mobility of the 10 mM, pH 6.1 buffer solution was 2.96×10^{-8} m^2/Vs, a difference of only 1.3 % from the data collected in the suspended microchannels (SI Figure 2).

The ability to produce precisely oriented, suspended microchannels may enable the development of more advanced microfluidic devices by eliminating spatial restrictions imposed by current 3D microfluidic fabrication

technology (e.g., confinement to a stack of planar channel arrangements). It has been demonstrated that the electrokinetic characteristics of these channels are nearly identical to those observed in conventional, planar BSG microchannels. Also, because the channels are freely suspended and can be fabricated on substrates with 3D features, the proposed technique may allow the in situ fabrication of inter-connecting channels which interface with existing microfluidic components (e.g., micropumps, valves, sensors).

4 Conclusions

The demonstrated ability to produce suspended microfibers with high yield and controlled diameter enabled their implementation as sacrificial structures in the production of microchannels. This fabrication sequence was optimized and suspended channels with smooth, hydrophilic walls were produced. The primary obstacle to this outcome was the difficulty associated with uniformly depositing a continuous, non-buckled layer of borosilicate glass around the PMMA structures. A multilayered sputtering process was developed and this improvement led to sustainable electroosmotic flow within the microchannels while increasing the magnitude of electrokinetic transport by a factor of 3. The functionality of these channels as electrokinetic conduits was further validated by demonstrating that the EK mobility of a common buffer solution in the suspended microchannels differs by only 1.3 % when compared with the measured mobility for a conventionally fabricated microchannel. As a further validation, PIV was used to measure the EK mobility of charged particles in a buffer solution in the suspended microchannels.

Acknowledgments This investigation was funded by the National Science Foundation NIRT Program (ECCS-0506941) and NSF PFI Program (EEC-0438604).

References

Anderson JR, Chiu DT, Jackman RJ, Cherniavskaya O, McDonald JC, Wu H, Whitesides SH, Whitesides GM (2000) Fabrication of topologically complex three-dimensional microfluidic systems in PDMS by rapid prototyping. Anal Chem 72:3158–3164

Beckers JL, Everaerts FM, Ackermans MT (1991) Determination of absolute mobilities, pK values and separation numbers by capillary zone electrophoresis: effective mobility as a parameter for screening. J Chromatogr 537:407–428

Bellan LM, Singh WP, Henderson PW, Porri TJ, Craighead HG, Spector JA (2009) Fabrication of an artificial 3-dimensional vascular network using sacrificial sugar structures. Soft Matter 5:1354–1357

Berry SM, Harfenist SA, Cohn RW, Keynton RS (2006) Characterization of micromanipulator-controlled dry spinning of micro- and sub-microscale polymer fibers. J Micromech Microeng 16:1825–1832

Berry SM, Pabba S, Crest J, Cambron SD, McKinley GH, Cohn RW, Keynton RS (2011a) Characterization and modeling of direct-write fabrication of microscale polymer fibers. Polymer 52: 1654–1661

Berry SM, Warren SP, Hilgart DA, Schworer AT, Pabba S, Gobin AS, Cohn RW, Keynton RS (2011b) Endothelial cell scaffolds generated by 3D direct writing of biodegradable polymer microfibers. Biomaterials 32:1872–1879

Blanco FJ, Agirregabiria M, Garcia J, Berganzo J, Tijero M, Arroyo MT, Ruano JM, Aramburu I, Mayora K (2004) Novel three-dimensional embedded SU-8 microchannels fabricated using a low temperature full wafer adhesive bonding. J Micromech Microeng 14:1047–1056

Carroll S, Crain MM, Naber JF, Keynton RS, Walsh KM, Baldwin RP (2008) Room temperature adhesive bonding of CE devices. Lab Chip 8:1564–1569

Chiu DT, Jeon NL, Huang S, Kane RS, Wargo CJ, Choi IS, Ingber DE, Whitesides GM (2000) Patterned deposition of cells and proteins onto surfaces by using three-dimensional microfluidic systems. PNAS 97(6):2408–2413

Chiu DT, Pezzoli E, Wu H, Stroock AD, Whitesides GM (2001) Using three-dimensional microfluidic networks for solving computationally hard problems. PNAS 98(6):2961–2966

Czaplewski DA, Verbridge SS, Kameoka J, Craighead HG (2004) Nanomechanical oscillators fabricated using polymeric nanofiber templates. Nano Lett 4(3):437–439

Doherty EAS, Meagher RJ, Albarghouthi MN, Barron AE (2003) Microchannel wall coatings for protein separations by capillary and chip electrophoresis. Electrophoresis 24:34–54

Harfenist SA, Cambron AD, Nelson EW, Berry SM, Isham AW, Crain MM, Walsh KM, Keynton RS, Cohn RW (2004) Direct drawing of suspended filamentary micro- and nanostructures from liquid polymers. Nano Lett 4(10):1931–1937

Hsieh S-S, Lin H-C, Lin C-Y (2006) Electroosmotic flow velocity measurements in a square microchannel. Colloid Polym Sci 284:1275–1286

Hsu TR (2002) MEMS and microsystems: design and manufacture. McGraw Hill, Boston

Hwang DJ, Choi TY, Grigoropoulos V (2004) Liquid-assisted femtosecond laser drilling of straight and three-dimensional microchannels in glass. Appl Phys A 79:605–612

Jo BH, Van Lerberghe LM, Motsegood KM, Beebe DJ (2000) Three-dimensional micro-channel fabrication in polydimethylsiloxane (PDMS) elastomer. J Micromech Microeng 9(1):76–81

Kameoka J, Orth R, Yang Y, Czaplewski D, Mathers R, Coates GW, Craighead HG (2003) A scanning tip electrospinning source for deposition of oriented nanofibres. Nanotechnology 14:1124–1129

Khan Malek CG, Das SS (1998) Adhesion promotion between poly(methylmethacrylate) and metallic surfaces for LiGA evaluated by shear stress measurements. J Vac Sci Technol B 16(6):3543–3546

Lide DR (ed) (1992) Handbook of Chemistry and Physics, 73rd edn. CRC, Roca Raton, FL

Nain AS, Wong JC, Amon C, Sitti M (2006) Drawing suspended polymer micro-/nanofibers using glass micropipettes. Appl Phys Lett 89:183105

Ren X, Bachman M, Sims C, Li GP, Allbritton N (2001) Electroosmotic properties of microfluidic channels composed of poly(dimethylsiloxane). J Chromatogr B 762:117–125

Verbridge SS, Edel JB, Stavis SM, Moran-Mirabal JM, Allen SD, Coates G, Craighead HG (2005) Suspended glass nanochannels coupled with microstructures for single molecule detection. J Appl Phys 97:124317

Wolf S, Tauber RN (1986) Silicon processing for the VLSI era. Lattice Press, Sunset Beach, CA